Frustrated phase separation in the momentum distribution of field-driven light-heavy Fermi-Fermi mixtures of ultracold atoms

H. F. Fotso,[1] J. Vicente,[2] and J. K. Freericks[1]

[1]*Department of Physics, Georgetown University, 37th and O Streets NW, Washington, DC 20057, USA*
[2]*Montgomery Blair High School, 51 University Boulevard East, Silver Spring, Maryland 20901, USA*

Time-of-flight images are a common tool in ultracold atomic experiments, employed to determine the quasimomentum distribution of the interacting particles. If one introduces a constant artificial electric field, then the quasimomentum distribution evolves in time as Bloch oscillations are generated in the system and then are damped, showing a complex series of patterns. In different-mass Fermi-Fermi mixtures, these patterns are formed from a frustrated phase separation in momentum space that is driven by Mott physics for large electric fields which stabilize them for long times.

PACS number(s): 03.75.Ss, 03.75.−b, 67.10.−j, 71.27.+a

I. INTRODUCTION

It is well known that systems driven out of equilibrium can sometimes develop persistent patterns in space and time which are metastable [1]. Can such metastable hydrodynamic instabilities persist in quantum fluids? Here we show an example which does in light-heavy Fermi-Fermi mixtures placed in a uniform artificial electric field [2].

Many different mixtures of ultracold atoms have already been made in the laboratory. We are interested in light-heavy mixtures of fermionic atoms, which include ^{6}Li and ^{40}K mixtures as the only possibility in the alkali-metal series. With the advent of alkaline-earth species, there are a number of possible Fermi-Fermi mixtures of different masses that can be achieved, as well as alkali-metal–alkaline-earth mixtures. In particular, experiments have already demonstrated such mixtures and have also examined the phenomenon of Bloch oscillations in optical lattices [3], so the experiment we describe below is feasible with experimental setups available today.

The equilibrium system of such a light-heavy mixture is described by the Falicov-Kimball model [4,5] [which can be obtained from the Hubbard model by fixing one of the spin species on the lattice (heavy) while the other is allowed to hop (light)]:

$$\mathcal{H}_{eq} = -\frac{1}{2\sqrt{d}} \sum_{\langle ij \rangle} J_{ij}^*(c_i^\dagger c_j + c_j^\dagger c_i)$$
$$- \mu \sum_i c_i^\dagger c_i + U \sum_i w_i c_i^\dagger c_i, \quad (1)$$

where $c_i^\dagger$ (c_i) is the creation (annihilation) operator for a light fermionic atom at site i, $w_i = 0,1$ is the occupation number operator of a heavy fermionic atom at site i, U is the s-wave interspecies interaction for doubly occupied lattice sites, $J_{ij}^* = J^*$ is the rescaled hopping amplitude between nearest-neighbor sites i and j of the light atoms and is used as the energy unit, and μ is the light-atom chemical potential. The system is initially in equilibrium at a temperature $T = 0.1$ (in units of J^*), which is experimentally feasible and is higher than the equilibrium critical temperature T_c for density wave formation or phase separation. A constant (artificial)

electric field $\mathcal{E}$ along the diagonal of the hypercubic lattice with $\mathcal{E} = \mathcal{E}(1,1,1,\dots)$ is then switched on at time $t = t_0$ and kept constant for subsequent times (this can be done using techniques in Ref. [2] or by using a light sheet to create a linear potential). In either case, the uniform electric field $\mathcal{E}(t)$ can be described by a vector-potential-only gauge with nonzero $\mathbf{A}(t)$ and $\mathcal{E}(t) = -\partial \mathbf{A}(t)/\partial t$, which is incorporated into the Hamiltonian via the Peierls substitution [6]:

$$J_{ij}^* \rightarrow J_{ij}^* e^{-i \int_{\mathbf{R}_i}^{\mathbf{R}_j} \mathbf{A}(t) \cdot d\mathbf{r}}. \quad (2)$$

This problem is similar to an interaction quench, where a parameter of the Hamiltonian is instantaneously switched from one constant value to the other, except here we have current flow, so thermalization is not so obvious [7]. We choose our units so that $c = e = \hbar = 1$.

To solve this problem, we consider the infinite-dimensional limit of the hypercubic lattice ($d \rightarrow \infty$ where the noninteracting density of states is a Gaussian [8]), and we use the dynamical mean-field theory (DMFT) [9–11], which is exact in infinite dimensions and provides a good approximation in finite dimensions at least if the temperature is not too low. In fact, a direct comparison of the DMFT and two-dimensional quantum Monte Carlo (QMC) results for the Falicov-Kimball model shows excellent agreement [12]. We ignore the trap in this work.

Each atomic species is chosen to have only one spin state, so we can ignore the intraspecies interaction. We consider the model at half filling for each atomic species ($\rho_{light} = \rho_{heavy} = 0.5$), where it obeys particle-hole symmetry.

II. METHODS

Our solutions are formulated in the Kadanoff-Baym-Keldysh formalism [13,14], in which observables are related to two-time Green's functions. The Green's functions are calculated for times on the Kadanoff-Baym-Keldysh contour which is discretized with a spacing Δt between consecutive times on the real branch while the imaginary branch has a spacing of $0.1i$, as shown in Fig. 1. The calculation is carried out for different values of Δt and is then extrapolated using a quadratic extrapolation to $\Delta t = 0$. The two-time
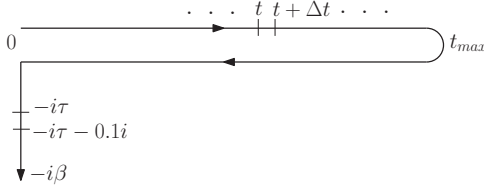
FIG. 1. Kadanoff-Baym-Keldysh contour for the nonequilibrium calculation of the two-time Green's function.

contour-ordered Green's function is defined by

$$G_{\mathbf{k}}^c(t,t') = -i \operatorname{Tr} \mathcal{T}_c e^{-\beta \mathcal{H}_{\mathrm{eq}}} c_{\mathbf{k}}(t) c_{\mathbf{k}}^\dagger(t') / \mathcal{Z}_{\mathrm{eq}}, \qquad (3)$$

with the operators in the Heisenberg representation. Here $\mathbf{k}$ is a quasimomentum vector in the Brillouin zone, $\beta = 1/T$ is the inverse temperature, and $\mathcal{Z}_{\mathrm{eq}}$ is the equilibrium partition function. (In the remainder of the paper, we will refer to quasimomentum as momentum.) In the presence of a constant electric field along the diagonal, the infinite-dimensional $\mathbf{k}$ space can be mapped onto a two-dimensional space characterized by a band energy $E(\mathbf{k})$ given by Eq. (4) and the negative of the band velocity projected onto the direction of the electric field $V(\mathbf{k})$ given by Eq. (5) as follows:

$$E(\mathbf{k}) = -\lim_{d\to\infty} \frac{J^*}{\sqrt{d}} \sum_{i=1}^d \cos(k_i), \qquad (4)$$

$$V(\mathbf{k}) = -\lim_{d\to\infty} \frac{J^*}{\sqrt{d}} \sum_{i=1}^d \sin(k_i), \qquad (5)$$

where the k_i's denote the coordinates of the momentum vector along the different axes of the hypercubic lattice. The two-time Green's function is calculated within the nonequilibrium DMFT where the self-energy keeps its time dependence but has no momentum dependence. This can be written as

$$\Sigma_{\mathbf{k}}(t,t') = \Sigma(t,t'). \qquad (6)$$

To calculate the local contour-ordered Green's function $G_{\mathrm{loc}}^c(t,t')$, a summation over momentum is necessary. We use the above mapping of the momentum onto the band energy $E(\mathbf{k})$ and band velocity $V(\mathbf{k})$ to reduce the summation to a double integration which is then calculated using a double-Gaussian integration (which employs at least 2500 total Gaussian integration points). The retarded and the lesser Green's functions, $G_{\mathbf{k}}^R(t,t')$ and $G_{\mathbf{k}}^<(t,t')$, defined by Eqs. (7) and (8), respectively, where $\{\cdot,\cdot\}_+$ denotes the anticommutator, are extracted from the local contour-ordered Green's function.

$$G_{\mathbf{k}}^R(t,t') = -i\,\theta(t,t')\operatorname{Tr}\mathcal{T}_c\, e^{-\beta\mathcal{H}_{\mathrm{eq}}} \{c_{\mathbf{k}}(t), c_{\mathbf{k}}^\dagger(t')\}_+ / \mathcal{Z}_{\mathrm{eq}}, \quad (7)$$

$$G_{\mathbf{k}}^<(t,t') = i\operatorname{Tr} e^{-\beta\mathcal{H}_{\mathrm{eq}}} c_{\mathbf{k}}^\dagger(t') c_{\mathbf{k}}(t) / \mathcal{Z}_{\mathrm{eq}}. \qquad (8)$$

The complete description of this solution is given in Ref. [11]. In addition, the algorithm also determines the local self-energy. From this, the $\mathbf{k}$-dependent retarded and lesser Green's functions, $G_{E(\mathbf{k}),V(\mathbf{k})}^R(t,t')$ and $G_{E(\mathbf{k}),V(\mathbf{k})}^<(t,t')$, are constructed by using Dyson's equation and the momentum-dependent noninteracting Green's function in the presence of a field. Note that these Green's functions are calculated in the

vector-potential-only gauge. In an experiment, one performs a time-of-flight measurement by suddenly dropping the trap and the lattice and allowing the atoms to expand before imaging them with resonant light. In this case, one actually measures the momentum distribution in the gauge [15]. Since many gauge choices are possible for a particular experiment, it is easier to represent the results in terms of the gauge-invariant Wigner distribution [16]. One can always reconstruct the experimental measurements by transforming from the gauge-invariant results to those in the particular gauge of the experiment. For the results presented here, this transformation involves a rotation at the Bloch frequency if the vector-potential gauge is employed in the experiment.

The gauge-invariant Wigner distribution is defined by

$$n_{E(\mathbf{k}),V(\mathbf{k})}(t) = -i G_{E(\mathbf{k}+\mathbf{A}(t)),V(\mathbf{k}+\mathbf{A}(t))}^<(t,t), \qquad (9)$$

but we actually calculate it from the ratio

$$n_{E(\mathbf{k}),V(\mathbf{k})}(t) = -i \frac{G_{E(\mathbf{k}+\mathbf{A}(t)),V(\mathbf{k}+\mathbf{A}(t))}^<(t,t)}{G_{E(\mathbf{k}+\mathbf{A}(t)),V(\mathbf{k}+\mathbf{A}(t))}^R(t,t)} \qquad (10)$$

since the equal-time retarded Green's function is simply the equal-time anticommutator which is equal to 1. We find this ratio expression to converge faster to the $\Delta t \to 0$ result since the retarded Green's function for a given discretization size often is not precisely equal to 1. The convergence is generally robust for small interactions and becomes harder for large interactions for which a finer time grid is required and for which the equilibrium result is difficult to reproduce. Moment sum rules extrapolated to $\Delta t = 0$ are used to gauge the accuracy of the final calculations.

In equilibrium, the noninteracting momentum distribution is given by the Fermi-Dirac distribution function. In nonequilibrium and with interactions, it is given by the gauge-invariant Wigner distribution $n_{\mathbf{k}}(t) = -i G_{\mathbf{k}+\mathbf{A}(t)}^<(t,t)$ [16], which depends only on the two aforementioned variables and is denoted $n_{E(\mathbf{k}),V(\mathbf{k})}(t)$. We use this quantity to track the occupation of states in momentum space as a function of time in different parameter regimes with both $E(\mathbf{k})$ and $V(\mathbf{k})$ between -3.9 and 4.0. This corresponds to the observable that would be measured in a time-of-flight experiment after postprocessing to make it gauge invariant.

III. RESULTS

Prior to the electric field being switched on, the system is in equilibrium at a temperature $T = 0.1$, and the Wigner distribution in momentum space is shown in the top panel of Fig. 2 for $U = 0.25$ and is similar for other values of U (but broadened). Vertical cuts through the data are plotted in the bottom panel for $V(\mathbf{k}) = 0$ as a function of $E(\mathbf{k})$ for various values of U. Note that despite its similarity to the Fermi-Dirac distribution of a noninteracting system (which is recovered for $U = 0.0$), this result includes the effects of interactions. The shaded area represents the range $[0.45, 0.55]$ over which $n_{\mathbf{k}}$ is plotted in the top panel. This same range is used for all of the following figures because it is the typical range over which the structures are seen in the long-time behavior. This 10% fluctuation in the signal should be measurable in current experiments.
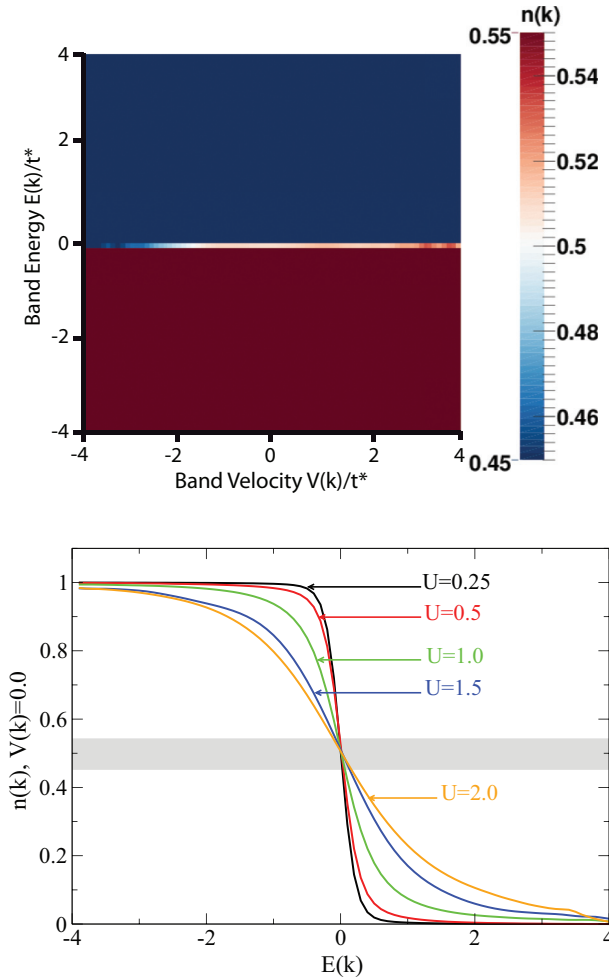
FIG. 2. (Color online) False-color image of the initial equilibrium Wigner distribution function at $T = 0.1$. The top panel plots $n_\mathbf{k}$ as a function of $E(\mathbf{k})$ and $V(\mathbf{k})$ for $U = 0.25$. The bottom panel shows $n_\mathbf{k}$ as a function of $E(\mathbf{k})$ for $V(\mathbf{k}) = 0.0$ and different values of U; the shaded area represents the range [0.45,0.55] over which $n_\mathbf{k}$ is plotted in the top panel. The deviation from the Fermi-Dirac distribution for $T = 0.1$ comes from the many-body effects of the interactions between the two types of atoms.

In the case of a noninteracting system, turning on a static electric field produces Bloch oscillations characterized in frequency space by Wannier-Stark ladders [17] and in momentum space by periodic oscillations with a period of $2\pi/\mathcal{E}$. These Bloch oscillations can be measured in the current or other observables [10,11,18,19]. The time evolution of the gauge-invariant Wigner distribution in momentum space is simply the rotation of the equilibrium configuration around the origin like a clock hand with an unchanged Fermi surface shape.

With the interspecies interaction turned on, the Bloch oscillations are gradually damped and decay towards zero, while the Wannier-Stark ladder in frequency space broadens and (for large electric fields) splits due to Mott transitions in each of the minibands [11]. The Joule heating resulting from the interaction increases the energy of the system at a rate given by $\mathcal{J}(t) \cdot \mathcal{E}$, with $\mathcal{J}(t)$ being the light-atom current [20]. This current eventually decays to zero as the isolated system

either thermalizes to an infinite temperature or gets stuck in a nonthermal nonequilibrium steady state. When thermalization occurs, all states are equally occupied, and we expect $\lim_{t\to\infty} n_{E,V} = 0.5$ for all (E, V) points [7]. Regardless of the thermalization scenario, the long-time limit is approached with the formation of specific patterns depending on the values of the electric field and the interspecies interaction. Two time scales characterize this development. One is related to the
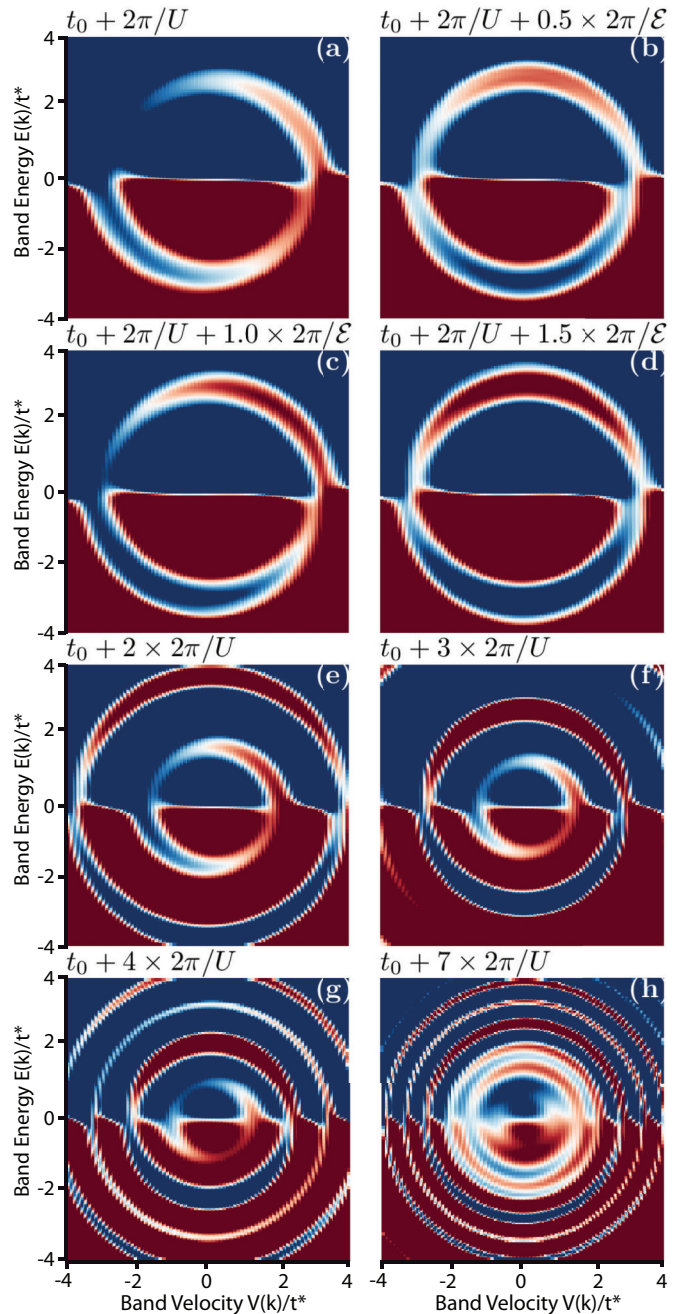

FIG. 3. (Color online) False-color images of the evolution of the gauge-invariant Wigner distribution in momentum space at different times for $\mathcal{E} = 2.0$ and $U = 0.25$. Each panel shows a snapshot of $n_\mathbf{k}(t)$ at an instant in time after the field is switched on (at t_0). (a)–(d) show the evolution for multiples of the time scale $2\pi/\mathcal{E}$, while (e)–(h) show multiples of the time scale $2\pi/U$.

Bloch oscillations, $T_{\text{Bloch}} = 2\pi/\mathcal{E}$, and the other is related to the collapse and revival of the Bloch oscillations for large fields and small interactions, $T_{\text{Beat}} = 2\pi/U$ [19,21,22]. We focus here on the large-field case ($\mathcal{E} = 2$), which has rich behavior that should be detectable in experiments.

Figure 3 shows different stages of the time evolution of the gauge-invariant Wigner distribution in the (E,V) plane for $\mathcal{E} = 2.0$ and $U = 0.25$. Figures 3(a)–3(d) probe the time scale T_{Bloch}, while Figs. 3(e)–3(h) probe the time scale T_{Beat}. This evolution is characterized by the formation of concentric ring-shaped disturbances with a region of high occupation and a region of low occupation that are spawned at the origin, $(E,V) = (0,0)$, and then move outward while at the same time oscillating around this origin (as an analogy to help picture the inherent motion that can be seen in the movies provided in the Supplemental Material, this is similar to a pebble being dropped into a pond). These disturbances are formed on a time scale of T_{Beat} reminiscent of the beats that are observed in the current as a function of time for large fields and small interaction values as previously illustrated in Ref. [11]. While they are moving away from the center, these disturbances also subtly rotate around the origin with a time scale of T_{Bloch}. Each new T_{Beat} time interval sees the formation of a new ring at the origin; they eventually pack closer and closer together at long times, making the region more homogeneous. Movies of the evolutions are shown in the Supplemental Material [23], where it is easier to see the additional rotations with period T_{Bloch}.

In Fig. 4, the evolution is observed for the same value of the electric field, $\mathcal{E} = 2.0$, and $U = 1.0$. In this case, the formation of the rings, their outward motion away from the origin, and their oscillation around the center occur on similar

time scales. As a result, the rings are no longer separated as in the case of smaller interactions. Instead, we see the formation of a spiral whose length grows with time. The spiral grows in length with the addition of a new layer after each T_{Beat} time step in a way analogous to the case of smaller interactions. The central region has a persistent pattern similar to the yin and yang symbol in Chinese culture.

When the interspecies interaction becomes larger, we see the formation in the middle of the spiral of a feature with one region of high occupation and one of low occupation (see Fig. 5). The formation of rings is initially reduced to that of

FIG. 5. (Color online) False-color image of the evolution of the gauge-invariant Wigner distribution with time for $\mathcal{E} = 2.0$ and $U = 3.0$. (a)–(d) show the behavior of the system on the time scale $2\pi/U$, while (e)–(h) show the time scale $2\pi/\mathcal{E}$.
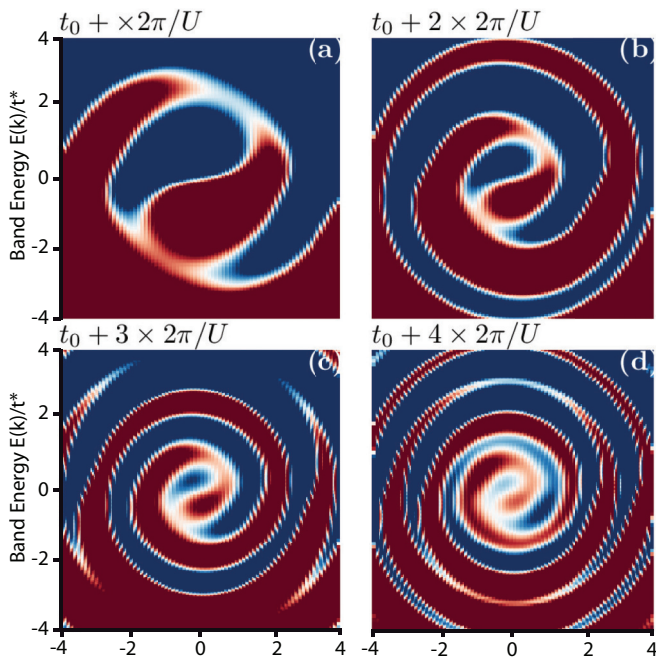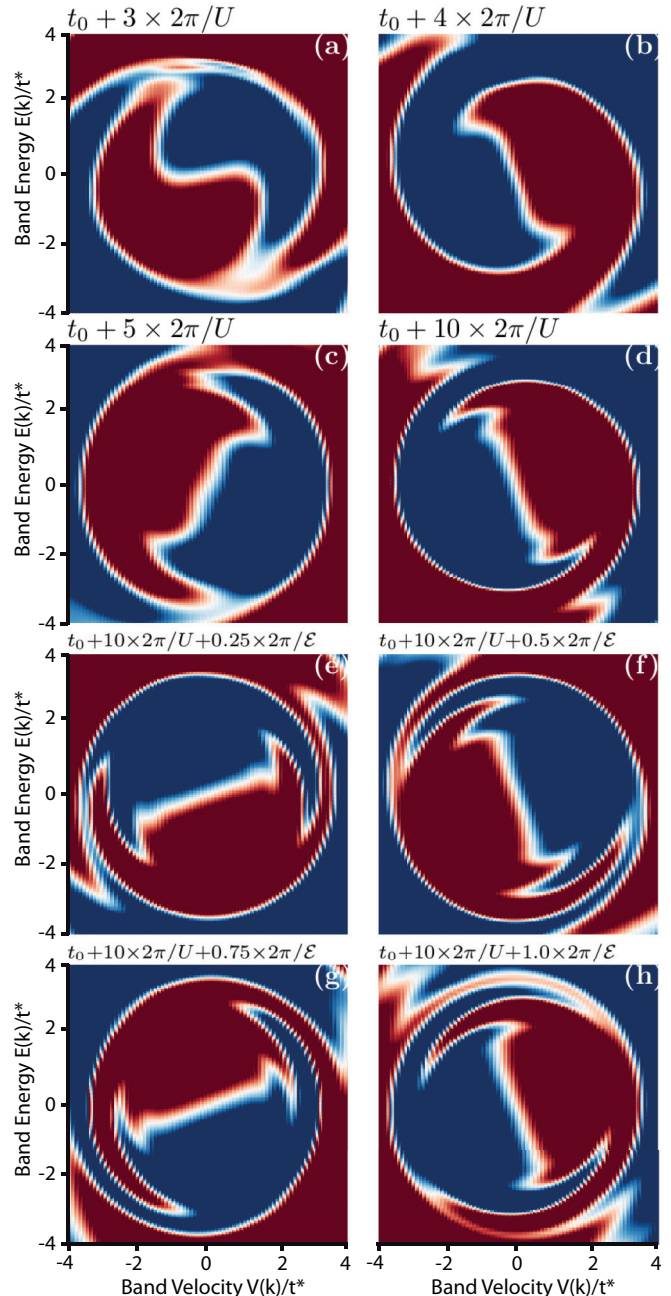

FIG. 4. (Color online) False-color images of the evolution of the gauge-invariant Wigner distribution in momentum space with time for $\mathcal{E} = 2.0$ and $U = 1.0$. Each panel shows a snapshot of $n_{\mathbf{k}}(t)$ at the corresponding instant in time.

small sharp edges on two well-defined regions, as shown in Figs. 5(a)–5(d). At even longer times, we observe no further changes to this central feature, and all the disturbances seem to be taking place outside of the simulated region. Throughout this evolution, the whole system rotates around the origin with a period of T_{Bloch}, as seen in Figs. 5(d)–5(h). The size of this region grows with the interaction, so that for even larger U, one would see a behavior analogous to the rotating Fermi surface of the noninteracting system at the Bloch frequency (when restricted to this 0.45–0.55 window).

The evolution of the gauge-invariant Wigner distribution shows the development of patterns that are robust and persistent up to long times. These patterns are most apparent when one focuses in on a window around the infinite-temperature thermal state where $n_{\mathbf{k}} = 0.5$. Initially, the Wigner distribution is between 0 and 1, and as the system heats up due to Joule heating, this interval is gradually reduced, so that at long times, the high-density region and the low-density region are shown with Wigner distributions focused between 0.45 and 0.55. The distribution will appear to saturate quickly if plotted for values smaller than 0.45 and larger than 0.55. Note that the diffraction pattern at the boundaries between different regions is due to the rendering algorithm of the plotting software [24] and is not a physical result. Movies showing the real-time evolution of the Wigner distribution for the different regimes described here are available in the Supplemental Material, along with a description of their production.

IV. CONCLUSION

We have studied the real-time evolution of the distribution function in the momentum space of a field-driven light-heavy Fermi-Fermi mixture and have found a surprising long-time stability of complex patterns in momentum space. The origin of this behavior lies in the tendency for these systems to phase separate when near a Mott phase [25,26]. Because

of the localizing effect of the field (which causes Wannier-Stark ladders of minibands with infinitesimal bandwidths), the Mott-like behavior is enhanced. For example, in the large-field regime even a small interaction can cause the Wannier-Stark-ladder-like peaks to split [11], creating Mott transitions in the minibands at interaction strengths much lower than the critical field needed in the absence of the field. But since the heavy particles must remain spatially homogeneous because they are not coupled to the field, the phase separation can occur only in momentum space as it is completely frustrated in real space. The frustrated phase separation is driven by the large mass difference, which enhances the tendency for phase separation; similar calculations for the Hubbard model show no such patterns [27]. What this implies is that the inherent tendency towards phase separation, which occurs when the interaction between the two species is large, is amplified in the presence of a large field. But because the heavy particles are immobile in the model (and move quite slowly in experiment), the system cannot phase separate in real space, so it must do so in momentum space, giving rise to the long-term stability of these systems. This nonequilibrium dynamical phase separation should be observable in cold-atom experiments with currently available technology.

[1] M. C. Cross and P. C. Hohenberg, Rev. Mod. Phys. **65**, 851 (1993).

[2] Y.-J. Lin, R. L. Compton, K. Jimnez-Garca, W. D. Phillips, J. V. Porto, and I. B. Spielman, Nat. Phys. **7**, 531 (2011).

[3] E. Wille, F. M. Spiegelhalder, G. Kerner, D. Naik, A. Trenkwalder, G. Hendl, F. Schreck, R. Grimm, T. G. Tiecke, J. T. M. Walraven, S. J. J. M. F. Kokkelmans, E. Tiesinga, and P. S. Julienne, Phys. Rev. Lett. **100**, 053201 (2008); T. G. Tiecke, M. R. Goosen, A. Ludewig, S. D. Gensemer, S. Kraft, S. J. J. M. F. Kokkelmans, and J. T. M. Walraven, *ibid.* **104**, 053202 (2010); F. M. Spiegelhalder, A. Trenkwalder, D. Naik, G. Kerner, E. Wille, G. Hendl, F. Schreck, and R. Grimm, Phys. Rev. A **81**, 043637 (2010); D. Naik, A. Trenkwalder, C. Kohstall, F. M. Spiegelhalder, M. Zaccanti, G. Hendl, F. Schreck, R. Grimm, T. M. Hanna, and P. S. Julienne, Eur. Phys. J. D **65**, 55 (2011); A. Trenkwalder, C. Kohstall, M. Zaccanti, D. Naik, A. I. Sidorov, F. Schreck, and R. Grimm, Phys. Rev. Lett. **106**, 115304 (2011).

[4] L. M. Falicov and J. C. Kimball, Phys. Rev. Lett. **22**, 997 (1969).

[5] C. Ates and K. Ziegler, Phys. Rev. A **71**, 063610 (2005).

[6] R. Peierls, Z. Phys. **80**, 763 (1933).

[7] H. F. Fotso, K. Mikelsons, and J. K. Freericks, Sci. Rep. **4**, 4699 (2014).

[8] W. Metzner and D. Vollhardt, Phys. Rev. Lett. **62**, 324 (1989).

[9] J. K. Freericks and V. Zlatić, Rev. Mod. Phys. **75**, 1333 (2003).

[10] J. K. Freericks, V. M. Turkowski, and V. Zlatić, Phys. Rev. Lett. **97**, 266408 (2006).

[11] J. K. Freericks, Phys. Rev. B **77**, 075109 (2008).

[12] A. Hu, J. K. Freericks, M. M. Maska, and C. J. Williams, Phys. Rev. A **83**, 043617 (2011).

[13] L. P. Kadanoff and G. Baym, *Quantum Statistical Mechanics* (Benjamin, New York, 1962).

[14] L. V. Keldysh, Zh. Eksp. Teor. Fiz. **47**, 1945 (1964) [Sov. Phys. JETP **20**, 1018 (1964)].

[15] H. Miyake, G. A. Siviloglou, C. J. Kennedy, W. C. Burton, and W. Ketterle, Phys. Rev. Lett. **111**, 185302 (2013).

[16] R. Bertoncini and A. P. Jauho, Phys. Rev. B **44**, 3655 (1991).

[17] G. H. Wannier, Phys. Rev. **100**, 1227 (1955); **101**, 1835 (1956); **117**, 432 (1960); Rev. Mod. Phys. **34**, 645 (1962).

[18] A. R. Kolovsky, Phys. Rev. Lett. **90**, 213002 (2003).

[19] F. Meinert, M. J. Mark, E. Kirilov, K. Lauber, P. Weinmann, M. Gröbner, and H.-C. Nägerl, Phys. Rev. Lett. **112**, 193003 (2014).

[20] M. Mierzejewski, J. Bonča, and P. Prelovšek, Phys. Rev. Lett. **107**, 126601 (2011).

[21] M. Greiner, O. Mandel, T. W. Hänsch, and I. Bloch, Nature (London) **419**, 51 (2002).

[22] A. Buchleitner and A. R. Kolovsky, Phys. Rev. Lett. **91**, 253002 (2003).

[23] See Supplemental Material at http://link.aps.org/supplemental/10.1103/PhysRevA.90.053630 for movies that show the full time evolution of the distribution function as a function of time for the cases where snapshots are provided in the main text. In addition, a description of the how the movies were produced is included.

[24] PARAVIEW, http://www.paraview.org/.

[25] J. K. Freericks, E. H. Lieb, and D. Ueltschi, Phys. Rev. Lett. **88**, 106401 (2002).

[26] J. K. Freericks, E. H. Lieb, and D. Ueltschi, Commun. Math. Phys. **227**, 243 (2002).

[27] K. Mikelsons, J. K. Freericks, and H. R. Krishnamurthy, in *2012 High Performance Computing Modernization Program Contributions to DOD Mission Success* (High Performance Computing Modernization Program of the Department of Defense, Lorton, VA, 2012), p. 219.